JMEPEG (2005) 14:553-562
DOI: 10.1361/105994905X64549

1059-9495/$19.00

Development of High Strain Rate Equations for Stainless Steels

R. Andersson, M. Syk, J. Powell, and C. Magnusson

(Submitted March 14, 2005; in revised form June 30, 2005)

The dynamic response of four types of stainless steel sheet was investigated at different strain rates from 10^{-2} up to 10^{3} s^{-1}. The results from the tensile tests were used to evaluate the parameters in three different multiplicative strain rate equations of the type used in crashworthiness calculations. A new type of sigmoid constitutive equation is proposed for one grade of stainless steel.

Keywords constitutive equations, high strain rate, stainless steel

1. Introduction

There is pressure on automotive manufacturers from different environmental groups to reduce the pollution from vehicles. One common way to achieve a lower pollutant level is to decrease the weight of the vehicle. This leads to a change in behavior of the automobile during a crash situation, so new designs and materials are needed to overcome this problem. One way to help the automotive industries to evaluate the occupant safety in a crash situation is through experimental tests. There are several independent research institutes and organizations that conduct these types of tests. One of the most important independent crash-impact test programs for automotives in Europe is the European New Car Assessment Program (Ref 1). This program is supported by Allgemeiner Deutscher Automobil-Club e V (ADAC), Alliance Internationale de Tourisme (AIT), Bundesministerium für Verkehr, Bau- und Wohnungswesen, Department for Transport, Local Government and the Regions (DTLR), Dutch Ministry of Transport, Public Works and Water Management, European Commission (EU), Fédération Internationale de l'Automobile (FIA), Generalitat de Catalunya, International Consumer Research and Testing, Ministère de l'Equipement, and the Swedish National Road Administration. The experimental tests made in this program are front impact, side impact, pedestrian impact, and head protection. For automotive manufacturers, these types of experimental tests are extremely costly. To decrease the cost, the crash tests are often reproduced virtually through software that simulates the behavior of the automotive structure during impact. To analyze different crash deformation modes in the computer environment, there is a requirement for accurate rate-dependent constitutive equations for the materials involved (Ref 2). These are often used in commercial finite element codes such as LS-Dyna (Ref 3) and PAM-CRASH (Ref 4), which are able to simulate crash behavior.

R. Andersson and **M. Syk,** Swedish Tool & Die Technology, Aurorum 8A, Luleå, Sweden; **J. Powell,** Laser Expertise, Acorn Park Industrial Estate, Nottingham NG7 2TR, England; and **C. Magnusson,** Volvo Cars Body Components, Olofström, Sweden. Contact e-mail: Roger@svenskverktygsteknik.com.

This study involves uniaxial tensile experiments to validate the response of stainless steel at high strain rates and to identify constitutive parameters for crashworthiness modeling.

One way to evaluate the experimental effective stress, strain, and strain-rate relationship for metallic sheets is through high strain-rate uniaxial tensile tests. These could be carried out at different temperatures but are commonly done at room temperature. The experimental procedure to assess a stress-strain curve at high strain rates can involve a number of test methods. Two of the more common methods are a hydraulic test machine configured for high strain-rate tests and a method that is known by the name of split-Hopkinson. These methods are described later in this article. This paper begins with an experimental program involving two high strain-rate tests methods each used on two stainless steels. The data from these tests is then used into the second half of the paper to identify which, if any, of the potentially suitable equations give a good fit to the experimental results over the range of strain rates investigated here. In the case of one of the materials, a new type of equation has been developed and found to give excellent results.

2. Material Specification

The materials in these studies are listed in Tables 1-3. All materials were tested in the as-received sheet condition. The mechanical data were evaluated through uniaxial tensile tests at a strain rate of 0.05 s^{-1} in a Dartec 50kN tensile testing machine. The extensometer was an Epsilon model number 3542-050M-025-ST. The European standard EN 10 002 defined the initial gauge length of the extensometer, which was proportional to the initial sample cross-section area.

3. Experimental Procedure and Results

3.1 High Strain Rate Hydraulic Machine Tests and Results

The first test method involved a hydraulic uniaxial tensile machine, VHS100, from Instron, capable of test speeds up 20 m/s (Ref 5). The materials tested with this method are sample numbers 1 and 2 in Table 1. All specimens were laser cut, and abrasive paper was used to polish the edges. The design of the specimens is shown in Fig. 1. The width w and thickness t were

Table 1 Stainless steel materials in this study and the test methods used to assess high strain rate

Type, EN	Trade name	Thickness, mm	Microstructure	Condition	Test method
1.4310	HyTens1000(a)	1.57	Austenitic-Martensitic	Temper rolled	High strain rate hydraulic machine
1.4362	SAF2304(b)	1.51	Duplex	Annealed	High strain rate hydraulic machine
···	Nanoflex(b)	0.51	Austenitic-precipitation hardenable	Annealed	Split-Hopkinson
1.4319	···	1.19	Austenitic	Annealed	Split-Hopkinson

(a) Trademark of Outokumpu Stainless, (b) Trademark of Sandvik Materials Technology

Table 2 Mechanical properties assessed from quasi-static uniaxial tensile tests at a strain rate of 0.05 s^{-1}

Type, EN	Trade name	Rp_{02}, MPa	Rm, MPa	A50, %
1.4310	HyTens1000(a)	639	1108	36
1.4362	SAF2304(b)	604	775	22
···	Nanoflex(b)	321	848	21
1.4319	···	256	605	54

(a) Trademark of Outokumpu Stainless, (b) Trademark of Sandvik Materials Technology

all measured with micrometer EA9202 to obtain the right cross-sectional area for all specimens. The width varied from 8.43 up to 9.22 mm. The force was measured by a piezo electric load cell GKT18 and the displacement through a built in sensor. Strains were measured with an extensometer connected to a Wheatstone bridge in half-bridge mode to minimize bending effects.

The test method was divided into two variants: low-speed tests up to 0.7 m/s and high-speed tests for 7.5 and 18 m/s.

3.2 Low-Speed Test Method

The specimen for low-speed tests up 0.7 m/s were mounted in the same rig used for the high-speed tests; the difference was that both ends of the specimen were fixed and no acceleration took place before the test started. To achieve a smooth acceleration, a slight tensile load of 50-75 MPa was applied on the specimen. The extension was measured by the extensometer and amplifier system.

The test system achieved the desired speed within the elastic region of the stress-strain curve.

3.3 High-Speed Test Method

The high-speed tests were done on the same machine as for the low-speed tests. The difference is at actuator speeds over 1 m/s the machine uses its proportional valve.

For low-speed tests the actuator is in close loop control, which means that the actual movement is compared with the command signal and corrections can be applied.

For high-speed testing the large proportional valves feed a voltage signal that leads to a corresponding opening of the valve that leads to movement of the actuator and this means that no correction of the actuator movement is possible. The testing at high speed means that the actuator has to accelerate before gripping the specimen and the grip must be designed for this purpose. This study was performed with an Instron fast jaw grip.

During the force measurement, the load signal from the Kistler load cell is affected by system resonance and one way to reduce this resonance signal is to use strain gauges on the tensile specimens. These strain gauges are adhesive bonded to the end of the specimens outside the waist area, see Fig. 2. The stress in this region is below the elastic-plastic transition during the test and consequently the strains are linearly elastic and this enables the signal to be used as a load signal.

The strain gauges (one on each side) are then connected to an amplifier as a double quarter bridge. The double quarter bridge configuration is used to minimize the effects of superimposed bending strains. A comparison of the load signal from the Kistler load cell and strain gauge is shown in Fig. 3.

For all tests the strain rate is stated. This strain rate is really the test parameter, as the actuator speed does not clearly describe the test condition.

The strain rate is not constant over the test as the strain is dependent on the elastic elongation in the specimen, machine backlash, etc. The strain-rate values in this study are calculated from test data according to this equation:

$$\dot{\varepsilon} = \frac{\varepsilon_{0.15} - \varepsilon_{0.01}}{t_{0.15} - t_{0.01}} \quad \text{(Eq 1)}$$

This calculated strain rate is an average of the strain rate over the plastic region before necking, which is the most interesting region for crash calculations.

The resulting high strain rate true stress-strain relationships for HyTens1000 and Duplex2304 are shown in Fig. 4.

This paper is primarily concerned with the fit of various equations to the data produced. For this reason, a detailed interpretation of the results presented in Fig. 4 would be out of place. However, it is worth noting that steel would generally be expected to respond with improved strength as the strain rate increases. This is because the mechanisms of plastic strain are, to some extent, time dependent. The results in Fig. 4 follow this expected trend.

3.4 Split-Hopkinson Test and Results

The split-Hopkinson test (Ref 6) was originally developed for pressure tests, which used the induced wave propagation in long elastic metallic bars to measure the pressure produced during dynamic events. This principle was later developed to measure tensile properties (Ref 7-9). A schematic description of the split-Hopkinson arrangement for evaluating material properties at high strain rates in compression and tension is shown in Fig. 5.

The setup consists of two long bars, an incident and transmitted bar, between which a specimen is sandwiched. For the tensile tests, a tube-like striker bar is put around incident bar and is accelerated by an air gun towards an anvil at the end of

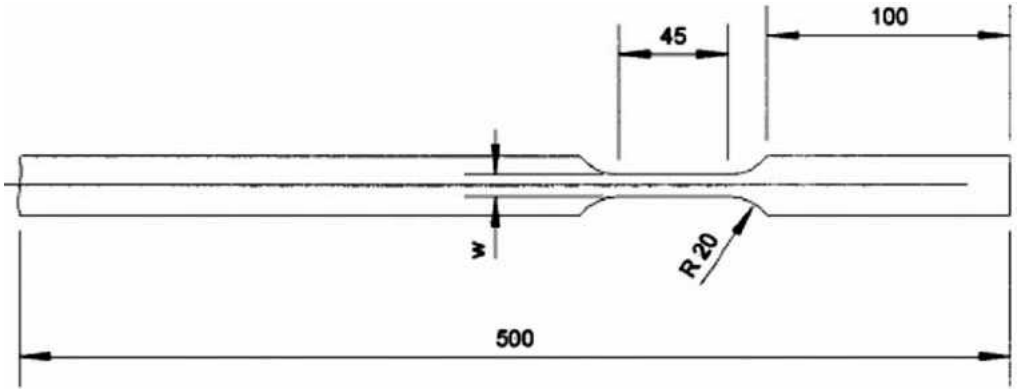

Fig. 1 Specimen design for high strain rate tests in the hydraulic high rate tensile machine

Fig. 2 Tensile specimen with an adhesive bonded strain gauge at the region with no waist. This enables the strain gauge to be used as load signal.

the incident bar. Thus, a tensile wave is generated in the incident bar and propagates until it reaches the edge where the specimen is clamped. A part of the incident wave reflects back to the incident bar while the rest propagates through the specimen into the transmitter bar. This wave creates displacements in the bars and can be measured through strain gauges. The true stress in the specimen is obtained by equilibrium of the forces in the transmitted bar and specimen as:

$$\sigma_s A_s = A_t E \varepsilon_t \rightarrow \sigma_s = \frac{A_t E \varepsilon_t}{A_s} \quad \text{(Eq 2)}$$

where A_t, E, and ε_t are the area, Young modulus, and true strain of the transmitted bar, respectively. A_s is the instantaneous cross-sectional area of the specimen, which is obtained from the constancy of volume in incompressible solids ($A_0 l_0 = A_s l_s$).

All strain gauges (measurement group CEA-06-250UW-350) on the bars are of the foil type with a gauge length of 6.35 mm. The signals from the gauges pass through the amplifiers and are finally sampled with a frequency of 2 MHz. The amplifiers (measurement group 2210A) have a bandwidth of 100 kHz.

3.5 Optimization of Specimen Geometry

The optimum specimen geometry was evaluated through several tests and investigations. Since specimens that deform at high strain rates have inertial and grip effects, which induce errors, the summation of the incident and reflected waves is not exactly equal to the transmitted wave.

$$\varepsilon_i + \varepsilon_r \neq \varepsilon_t \quad \text{(Eq 3)}$$

This means that the error from the geometry and grip can be measured as the amount of discrepancy as in Eq 4:

$$\text{Spec error } (\%) = \frac{\varepsilon_i + \varepsilon_r - \varepsilon_t}{\varepsilon_i} \cdot 100 \quad \text{(Eq 4)}$$

The discrepancies between the strain gauges (A + B) shown in Fig. 5 can be used to determine the specimen error. Results for different specimen gauge lengths are shown in Fig. 6. Figure 6 showed that the induced error decreases with decreasing gauge length. From this graph, it was decided that the gauge length should be 4 mm. After this decision several new specimens with gauge widths from 4 to 12 mm in steps of 1 mm were used. The specimen error for different widths is shown in Fig. 7. Figure 7 clearly indicates that the minimum error is possible at a gauge width of 7 mm. From the results shown in Fig. 6 and 7, the geometry was fixed for this study, shown in Fig. 8. All specimens were manufactured by electric wire discharge, which is assumed to have very small impact on the material property. The strain rate values in this study are calculated from test data according to this equation:

$$\dot{\varepsilon} = \frac{\varepsilon_{0.15} - \varepsilon_{0.01}}{t_{0.15} - t_{0.01}} \quad \text{(Eq 5)}$$

This calculated strain rate is an average of the strain rate over the plastic region before necking, which is the most interesting region for crash calculations.

The resulting high strain rate true stress-strain relationship for the Nanoflex materials and En1.4319 are shown in Fig. 9. The experimental results for Nanoflex show the unusual result that the strength level decreases with increasing strain rates and that dynamic recovery and strain rate softening occurs. For the EN1.4319 the material behavior was more as expected, i.e., increasing stress levels with increasing strain rates.

3.6 Fitting the Experimental Data to Suitable Mathematical Functions

The finite element method (FEM) often uses high strain-rate data in numerical calculation for impact situations and crashworthiness. The relationship between uniaxial true stress and strain at high strain rates can usually be implemented in the FEM software in two ways; one way is to write in points on the material curves for the different strain rates and the program interpolates between these points. The other way to implement experimental results is to fit the data to a mathematical expression.

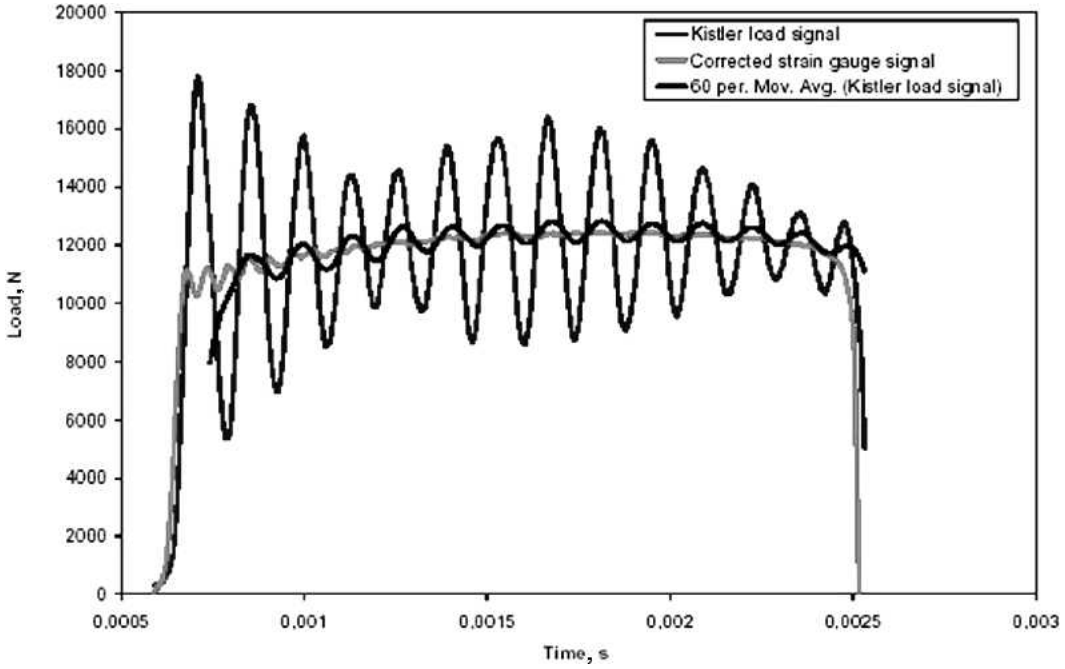

Fig. 3 Time-load curves showing the difference in ringing when comparing the signal from the load cell and strain gauges placed on the specimen

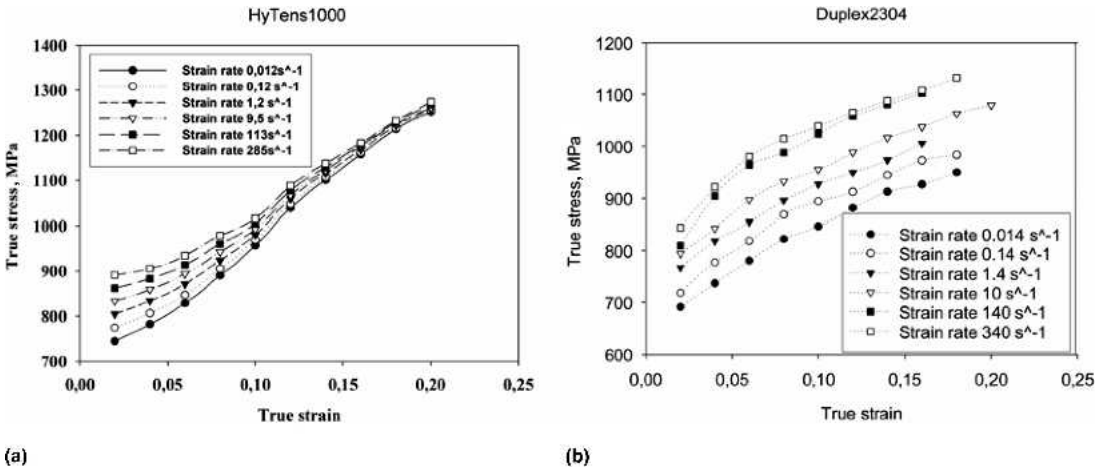

Fig. 4 True stress-strain relationship at different strain rates for (a) HyTens1000 and (b) Duplex2304

Table 3 Nominal chemical compositions for the materials in this study

Type, EN	Trade name	C	N_2	Si	Mn	P	S	Cr	Ni	Mo	Cu	Ti	Al
1.4310	HyTens1000(a)	0.1	0.02	0.8	1.2	0.02	0.002	17	7	0.3	0.2	0.001	0.003
1.4362	SAF2304(b)	0.02	0.1	0.4	1.5	0.02	0.002	23	4.8	0.3	0.3	0.001	0.003
⋯	Nanoflex(b)	0.02	⋯	0.5	0.5	0.02	0.005	12	9	4	2	0.9	0.4
1.4319	⋯	0.04	0.05	0.3	1.3	0.02	0.003	18	8	0.3	0.3	0.005	0.003

(a) Trademark of Outokumpu Stainless, (b) Trademark of Sandvik Materials Technology

A number of workers in the field have developed the mathematical functions we will now try to fit to the experimental data. Most of the early work involved the development of stress-strain equations that were appropriate to very low strain rates. Subsequent workers developed functions, which corrected the basic equations for higher strain rates. This correction is achieved by multiplying the basic stress-strain equation by the correcting function.

For more stable grades of stainless steel (Duplex and Nanoflex in this case) Swifts equation (Ref 10) works very well at low strain rates and is expressed as follows:

$$\bar{\sigma} = K(\varepsilon_0 + \bar{\varepsilon})^n \quad \text{(Eq 6)}$$

where K, ε_0, and n are constants.

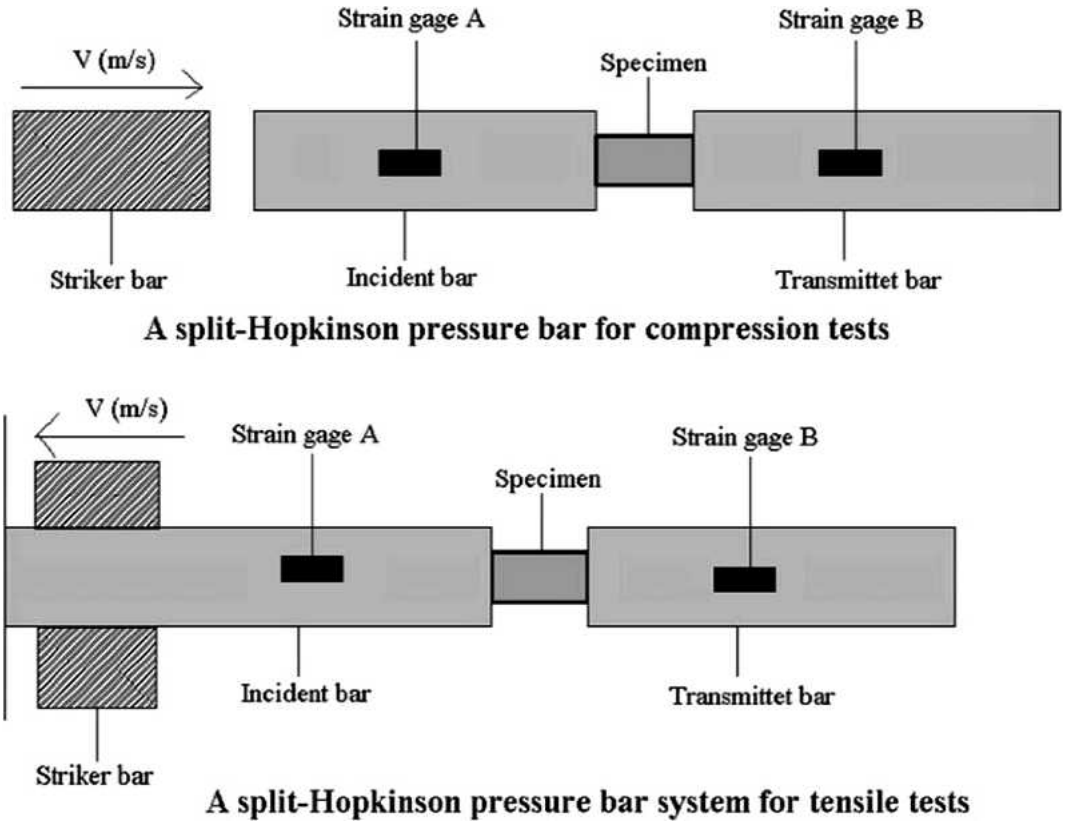

Fig. 5 Split-Hopkinson set up for evaluation of material properties at high strain rate in compression or tension

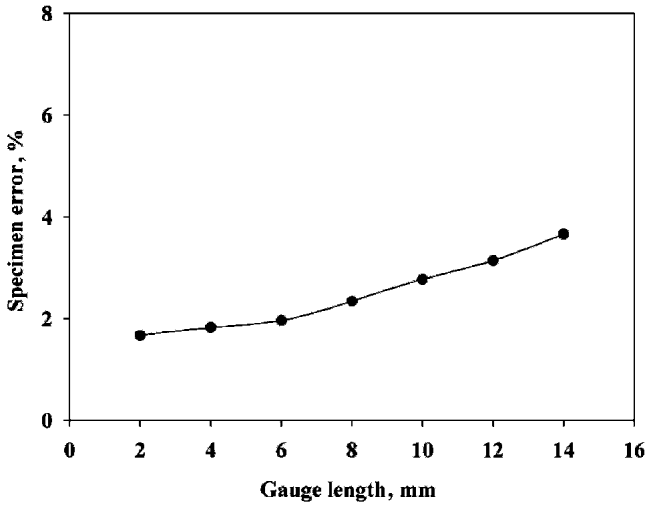

Fig. 6 Induced error from specimen setup against gauge length

Table 4 Multiplicative strain rate flow functions

Model name	Equation
Cowper-Symonds (Ref 13)	$1 + \left[\frac{\dot{\varepsilon}}{\mathrm{D}}\right]^{\mathrm{M}}$
Johnson-Cook (Ref 14)	$1 + \mathrm{D} \cdot \ln\left(\frac{\dot{\varepsilon}}{\dot{\varepsilon}_{\mathrm{ref}}}\right)$
Jones (Ref 15)	$1 + \left[\frac{(\varepsilon_{\mathrm{u}} - \varepsilon_{\mathrm{y}})\dot{\varepsilon}}{\mathrm{D} \cdot (\varepsilon_{\mathrm{u}} - \varepsilon) + E \cdot (\varepsilon - \varepsilon_{\mathrm{y}})}\right]^{\mathrm{M}}$

Table 5 Evaluated constants of the multiplicative strain rate flow functions for HyTens1000

Cowper-Symonds multiplicative strain rate function combined with Ludwigson constitutive equation									Curve fit parameter
K	n	B	A	C	Q	D	M		R^2_{adj}
4748	1.1	4.53	230.31	529.79	−0.02	935.80	637.36		0.99766
Johnson-Cook multiplicative strain rate function combined with Ludwigson constitutive equation									
K	n	B	A	C	Q	D			
3602	0.49	0.31	0.099	0.41	−2.02	0.056			0.99283
Jones multiplicative strain rate function combined with Ludwigson constitutive equation									
K	n	B	A	C	Q	D	E	M	
9590	0.84	0.31	2.63	137.13	−1.67	45618	3513	9.98	0.99174

The equation is more complex for meta-stable materials, which undergo a strain induced microstructural change from austenite to martensite (HyTens1000 and EN1.4319 in this case). In an earlier study (Ref 11), it was found that the Ludwigson equation (Ref 12) gave an excellent curve fit for this type of material. The equation is expressed as follows:

$$\overline{\sigma} = K\overline{\varepsilon}^{n} \cdot [1 - (1 + (e^{-B}/A)^{-1})] + C \cdot [1 + (e^{-B}/A)]^{-Q} \qquad \text{(Eq 7)}$$

where K, n, B, A, C, and Q are constants.

These two equations will be used as the basis of the curve fit for their respective steel grades. The basic equations need to be multiplied by a correction function that makes them more accurate for high strain rates. These are a number of such correction functions in the literature, and we will compare the accuracy of three of them. The correction functions are generally known as multiplicative strain rate flow functions and are referred to by the name of the people who developed them. In the following analysis, Eq 6 (for the Duplex and Nanoflex materials) and Eq 7 (for the HyTens1000 and En1.4319 materials) will each be multiplied by each of the multiplicative strain rate flow functions given in Table 4.

With the basic equations and the different correcting functions known, we need to give values to the constants in the equations. The stress-strain data for the lowest strain rate tests give us the values of K, n, D, etc. Then we can assess the fit of the resulting curve to the data at higher strain rates. The experimentally derived values of the constants for the equations are given in Tables 5-8.The curve fit parameter is the adjusted coefficient R^2_{adj} (Ref 16). This is a measure of how well the regression model describes the data and takes account of the number of independent variables, which reflects the degree of freedom. This parameter should be over 0.993 to get an acceptable fit of the equation to the experimental data.

To verify these evaluated parameters, the multiplicative strain-rate functions are now graphically compared with the stress-strain data at the highest tested strain rate. The results are shown in Fig. 10-13. Figures 10-13 show that three of the stainless grades have an acceptable curve fit from one of the multiplicative strain rate functions. This is Johnson-Cook for the Duplex and Nanoflex grades and Cowper-Symonds for the EN1.4319 grade.

For the HyTens grade, there is a need for better equation that describes the materials behavior at higher strain rates. For this

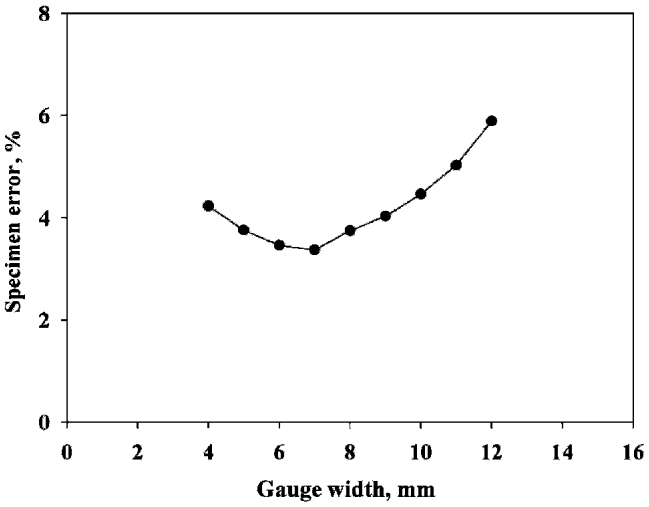

Fig. 7 Induced error from specimen setup against gauge width

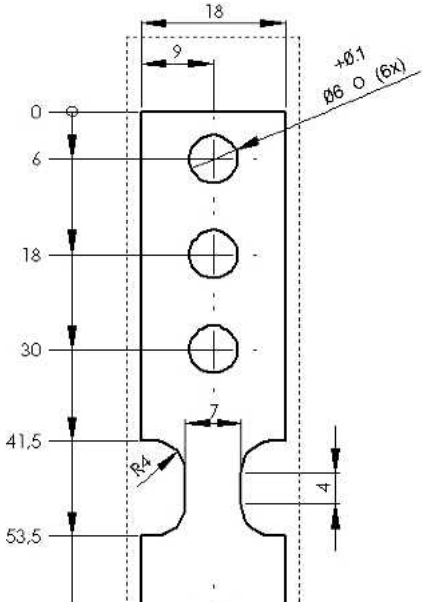

Fig. 8 Optimized specimen geometry for the tensile split-Hopkinson pressure bars tested in this study

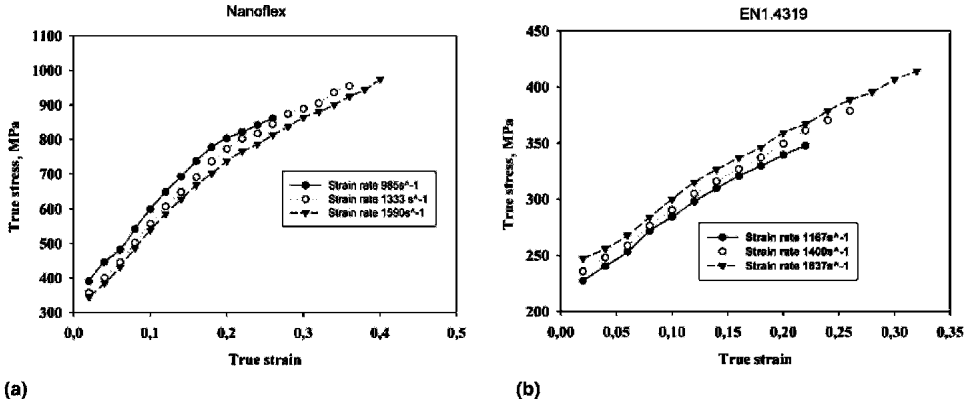

Fig. 9 True stress-strain relationship at different strain rates for (a) Nanoflex and (b) EN1.4319

Table 6 Evaluated constants of the multiplicative strain rate flow functions for Duplex2304

Cowper-Symonds multiplicative strain rate function combined with Swifts constitutive equation						Curve fit parameter
K	**ε_0**	**n**	**D**	**M**		**R^2_{adj}**
1397	0.0429	0.255	8728.59	0.279		0.99370
Johnson-Cook multiplicative strain rate function combined with Swifts constitutive equation						
K	ε_0	n	D			
1397	0.0429	0.255	0.0029			0.99411
Jones multiplicative strain rate function combined with Swifts constitutive equation						
K	ε_0	n	D	E	M	
1397	0.0429	0.255	12.97	22.03	0.65	0.99388

Table 7 Evaluated constants of the multiplicative strain rate flow functions for Nanoflex

Cowper-Symonds multiplicative strain rate function combined with Swifts constitutive equation						Curve fit parameter
K	**ε_0**	**n**	**D**	**M**		**R^2_{adj}**
1653	0.0387	0.515	4202	10.50		0.99041
Johnson-Cook multiplicative strain rate function combined with Swifts constitutive equation						
K	ε_0	n	D			
1660	0.0396	0.519	−0.205			0.99274
Jones multiplicative strain rate function combined with Swifts constitutive equation						
K	ε_0	n	D	E	M	
300	0.0909	1.1	782	824	11.43	0.99332

Table 8 Evaluated constants of the multiplicative strain rate flow functions for EN1.4319

Cowper multiplicative strain rate function combined with Ludwigson constitutive equation									Curve fit parameter
K	**n**	**B**	**A**	**C**	**Q**	**D**	**M**		**R^2_{adj}**
480	1.42	−0.066	0.0000018	0.0000068	−1.34	−682.81	−7		0.99017
Johnson-Cook multiplicative strain rate function combined with Ludwigson constitutive equation									
K	n	B	A	C	Q	D			
480	1.42	−0.066	0.0000018	0.0000068	−1.34	−0.25			0.99115
Jones multiplicative strain rate function combined with Ludwigson constitutive equation									
K	n	B	A	C	Q	D	E	M	
3075	1.1	0.46	5.10	−1173	329.26	7.19	1412.47	0.919	0.98934

Table 9 Evaluated constants of the additive exponential decay strain rate function between strain rates of 0.012 and 0.12 s^{-1}

$$\Delta\bar{\sigma}\dot{\varepsilon} = \ln\left(\frac{\dot{\varepsilon}}{\dot{\varepsilon}_{ref}}\right) \cdot a \cdot e^{-b\varepsilon}$$

		Curve fit parameter
a	**b**	**R^2_{adj}**
20.67	15.95	0.9512

grade, the increase in strength with increasing strain rates is not uniform over the whole stress-strain relationship. This is clear from Fig. 4, which shows that the stress-strain curves for different strain rates converge as the true strain is increased. The only multiplicative strain rate function that takes strain levels into account is the one proposed by Jones, but this does not give good curve fit for the HyTens grade.

We need to develop a new correction function for the Ludwigson equation in the case of the HyTens material. Using the data from Fig. 4, we can produce Fig. 14, which describes the convergence of the curves in Fig. 4. Figure 14 shows that the change in stress levels over the strain range is a typical exponential decay function. An exponential decay function describing the strain rate effect can now be evaluated to model the stress increase with increasing deformation speed. This proposed equation is simply a standard exponential decay function multiplied by a logarithmic function that incorporates strain rate difference, i.e.,

$$\Delta\bar{\sigma}_{\dot{\varepsilon}} = \ln\left(\frac{\dot{\varepsilon}}{\dot{\varepsilon}_{ref}}\right) \cdot a \cdot e^{-b\varepsilon} \quad \text{(Eq 8)}$$

where a and b are constants. In this study $\dot{\varepsilon}_{ref}$ is 0.012 s^{-1}, which is equal to the lowest tested strain rate for HyTens1000.

The constants in this equation were assessed from the data in Fig. 14, and the resulting fit is shown in Fig. 15 and tabulated in Table 9. If we now add this function (Eq 8) to the Ludwigson equation (Eq 7) we can carry out the curve fitting routine as before. The new constants for the equation is given in Table 10, and the curve fit results at strain rates of 1.2, 9, and

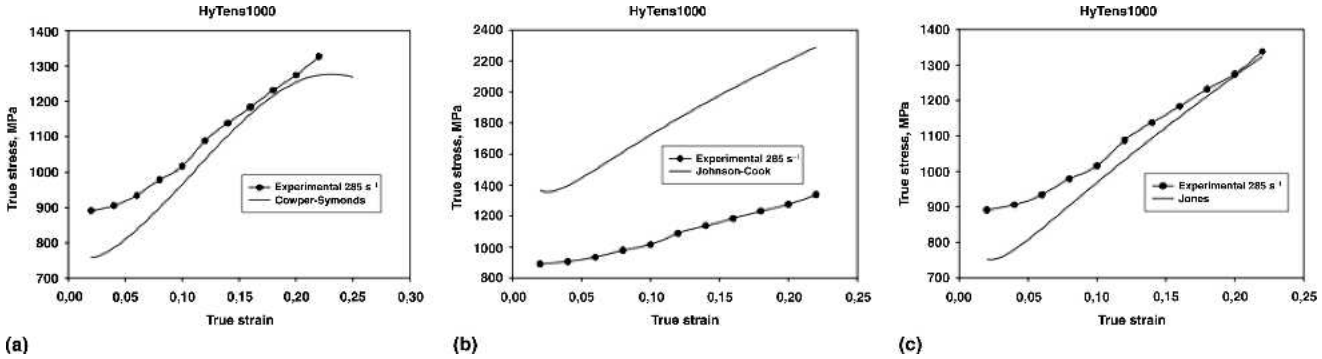

Fig. 10 Multiplicative equations in this study fit at a strain rate of 285 s^{-1} to the true stress-strain curve of HyTens1000 (a) Cowper-Symonds (Ref 13), (b) Johnson-Cook (Ref 14), and (c) Jones (Ref 15)

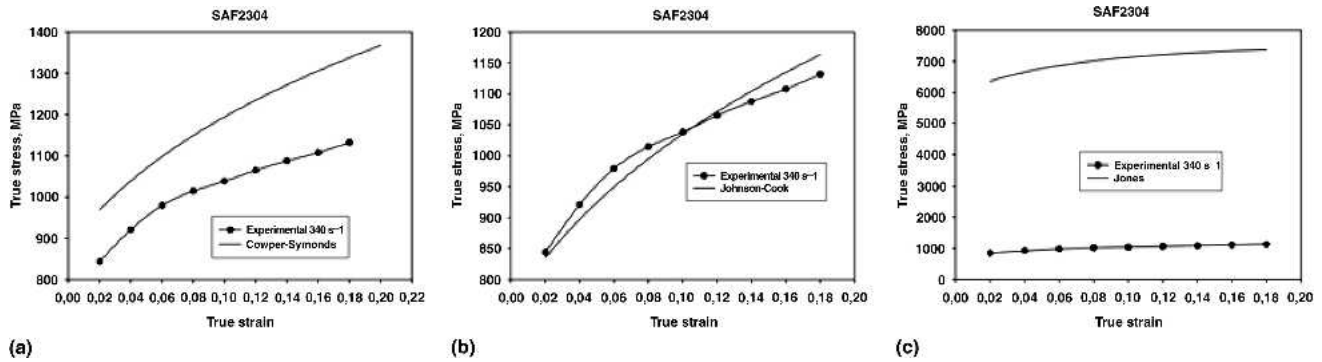

Fig. 11 Multiplicative equations in this study fit at a strain rate of 340 s^{-1} to the true stress-strain curve of Duplex2304 (a) Cowper-Symonds (Ref 13), (b) Johnson-Cook (Ref 14), and (c) Jones (Ref 15)

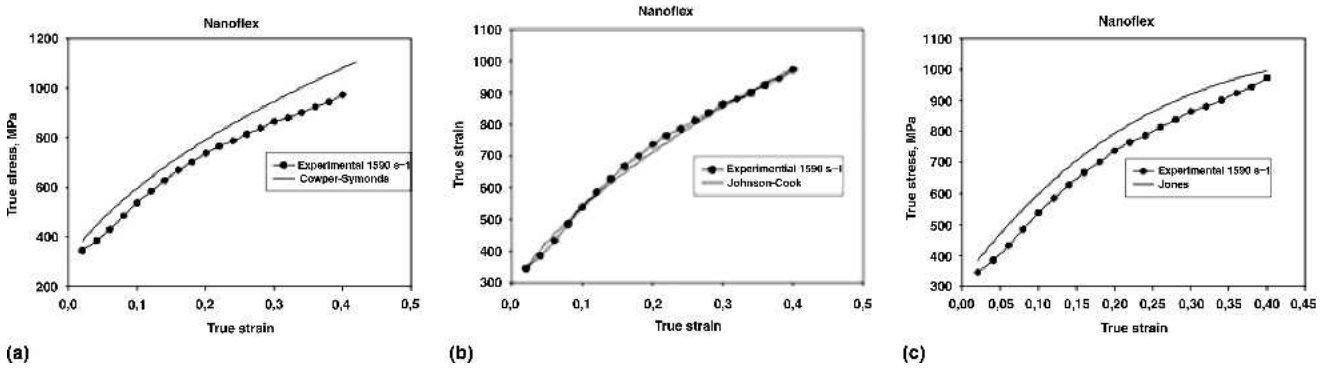

Fig. 12 Multiplicative equations in this study fit at a strain rate of 1590 s^{-1} to the true stress-strain curve of Nanoflex (a) Cowper-Symonds (Ref 13), (b) Johnson-Cook (Ref 14), and (c) Jones (Ref 15)

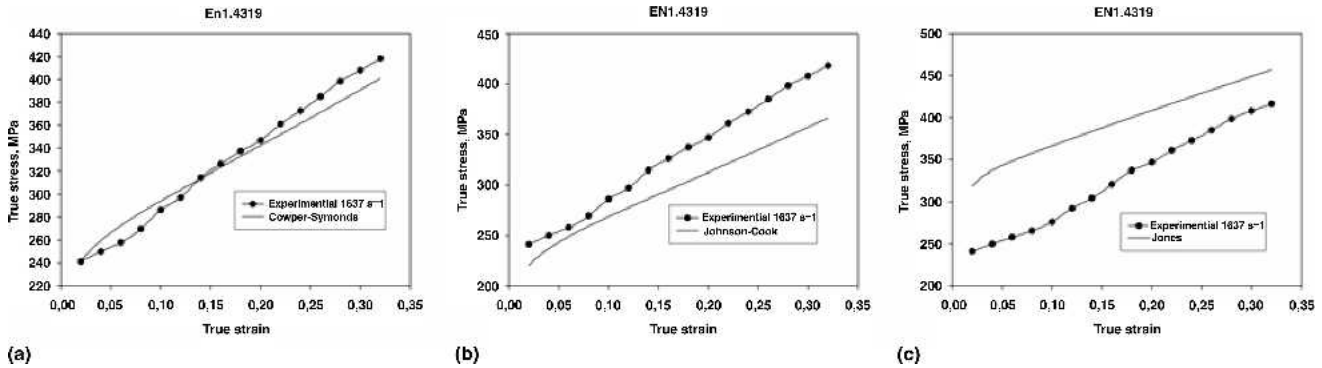

Fig. 13 Multiplicative equations in this study fit at a strain rate of 1637 s^{-1} to the true stress-strain curve of EN1.4319 (a) Cowper-Symonds (Ref 13), (b) Johnson-Cook (Ref 14), and (c) Jones (Ref 15)

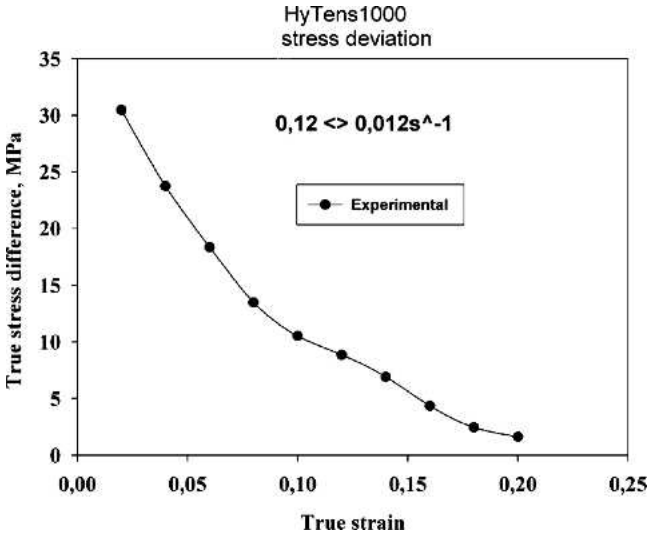

Fig. 14 True stress difference over the strain region between the strain rate of 0.012 and 0.12 s^{-1}

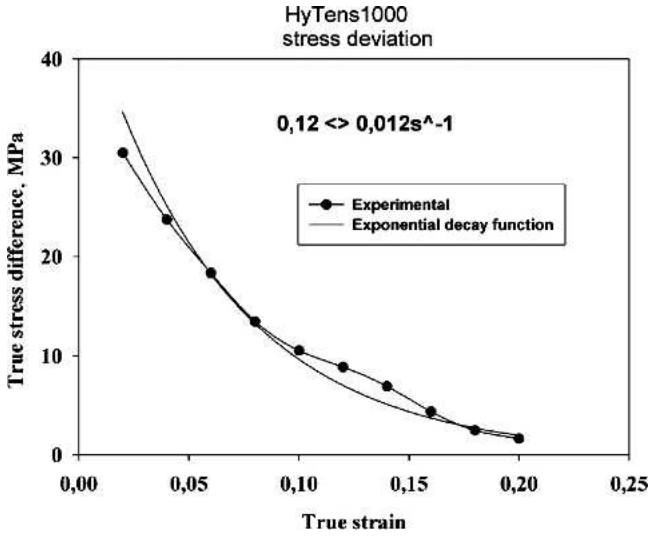

Fig. 15 Additive exponential decay strain rate function fits the stress difference over the strain region between strain rates of 0.12 and 0.012 s^{-1}

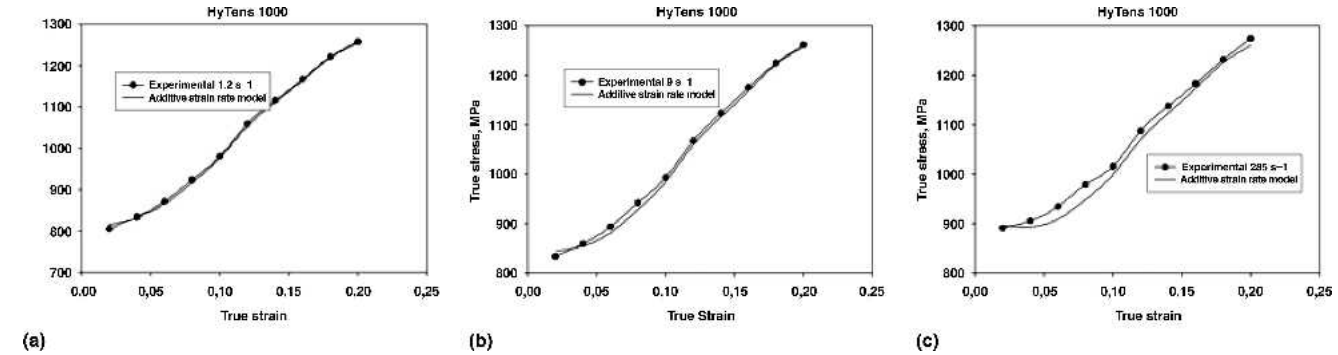

Fig. 16 Proposed additive exponential strain rate function in this study fits at different strain rates to HyTens1000 (a) 1.2 s^{-1}, (b) 9 s^{-1}, (c) 285 s^{-1}

Table 10 Evaluated constants of the multiplicative strain rate flow functions for HyTens1000

Cowper-Symonds multiplicative strain rate function combined with Ludwigson constitutive equation						Curve fit parameter		
K	**n**	**B**	**A**	**C**	**Q**	**n**	**b**	R^2_{adj}
2728	0.59	0.29	0.0000104	0.000043	−1.28	20.67	15.95	0.99793

285 s^{-1} are given in Fig. 16. The results in Fig. 16 show clearly that the proposed exponential strain-rate function added to the reference curve gives a much better prediction of the true stress-strain behavior at different strain rates than the multiplicative strain-rate functions used earlier in this paper.

4. Conclusion

This paper has demonstrated that a combination of Swifts equation and the Johnson-Cook multiplicative strain-rate function gives a good curve fit at high strain rates for the Duplex (SAF 2304) and Nanoflex materials tested here. A similarly good fit with experimental results was achieved using the Ludwigson equation and the Cowper-Symonds multiplicative strain rate function for stainless steel EN1.4319. It was not possible to get a good curve fit for HyTens1000 material, and a new equation was developed to achieve this aim. The new equation involves adding an exponential function to the Ludwigson equation and the resulting curve fit is extremely good.

References

1. http://www.euroncap.com/index.php (20030312)
2. *Metalworking Science and Engineering,* E.M. Mielnik, Ed., McGraw-Hill Inc., 1991.
3. http://www.ls-dyna.com (20030312)
4. http://www.esi-group.com (20030312)
5. http://www.instron.com/wa/home/default.aspx (20030522)
6. B. Hopkinson, A Method of Measuring the Pressure Produced in the

Detonation of High Explosives or by the Impact of Bullets, *Philos. Trans. R. Soc. London A,* Vol 213, 1914, p 437-456
7. J. Harding, E.O. Wood, and J.D. Campbell, Tensile Testing of Materials at Impact Rates of Strain, *J. Mech. Eng. Sci.,* Vol 2, 1960, p 88-96
8. U.S. Lindholm and L.M. Yeakley, High Strain Rate Testing: Tension and Compression, *Exp. Mech.,* Vol 8, 1968, p 1-9
9. G.H. Staab and A. Gilat, A Direct-Tension Split Hopkinson bar for High Strain Rate Testing, *Experimental Mechanics,* Vol 31, 1991, p 232-235
10. H.W. Swift, *J. Mech. Phys. Solids,* 1952, p 1-8
11. R. Andersson, "Effects of Composition and the Production Process on Formability of Austenitic Stainless Steels," Licentiate Thesis, Luleå University of Technology, Div. Materials Processing, Luleå, Sweden, 1999
12. D.C. Ludwigson, *J. Iron Steel Inst.,* Vol 207, 1969, p 413-422
13. P.S. Symonds, Survey of Methods of Analysis for Plastic Deformation of Structures under Dynamic Loading, Report BU/NSRDC, Brown University, Providence, RI, 1967
14. G.R. Johnson and W.H. Cook, A Constitutive Model and Data for Metal Subjected to Large Strains, High Strain Rates and High Temperatures, *Proc. 7th Symp. On Ballistics*, The Hague, The Netherlands, 1983, p 541-547
15. N. Jones, Some Comments on the Modelling of Materials Properties for Dynamic Structural Analysis, *Inst. Conf Mech. Prop. Materials at High Rates of Strain,* Inst. Phys. Conf. Ser. 102, Session 109, Oxford, UK, 1989
16. Sigmaplot 4.0 for Windows, SPSS Inc.